Geophysical Research Letters

RESEARCH LETTER
10.1029/2022GL099140

India (Tethyan Himalaya Series) in Central Myanmar: Implications for the Evolution of the Eastern Himalayan Syntaxis and the Sagaing Transform-Fault System

Myo Min[1,2], Lothar Ratschbacher[1], Leander Franz[3], Bradley R. Hacker[4], Eva Enkelmann[5], Eko Yoan Toreno[1], Birk Härtel[1], Bernd Schurr[6], Marion Tichomirowa[1], and Jörg A. Pfänder[1]

[1]Geowissenschaften, TU Bergakademie Freiberg, Freiberg, Germany, [2]Geology Department, University of Mandalay, Mandalay, Myanmar, [3]Mineralogisch-Petrologisches Institut, Universität Basel, Basel, Switzerland, [4]Geological Sciences, University of California, Santa Barbara, CA, USA, [5]Department of Geosciences, University of Calgary, Calgary, AB, Canada, [6]German Research Center for Geoscience, Potsdam, Germany

Abstract In the Katha Range of central Myanmar, lithologic tracers and pressure-temperature-deformation-time data identify Cambro-Ordovician, Indian-affinity Tethyan Himalaya Series, located ~700 km from their easternmost outcrop in S-Tibet, and ~450 km from Himalayan rocks in the Eastern Himalayan Syntaxis. Metamorphism began at ~65 Ma, peaked at ~45 Ma (~510°C, 0.93 GPa), and exhumation/cooling (~25°C/Myr) occurred until ~30 Ma in a subduction-early collision tectonic setting. When the Burma microplate—part of the intra-Tethyan Incertus arc—accreted to SE-Asia, its eastern boundary, the southern continuation of the Indus-Yarlung suture (IYS), was reactivated as the Sagaing fault (SF), which propagated northward into Indian rocks. In the Katha rocks, this strike-slip stage is marked by ~4°C/Myr exhumation/cooling. Restoring the SF system defines a continental collision-oceanic subduction transition junction, where the IYS bifurcates into the SF at the eastern edge of the Burma microplate and the Jurassic ophiolite-Jadeite belts that include the Incertus-arc suture.

Plain Language Summary Central Myanmar hosts rocks typical for the northernmost continental crust of the Indian continent—the Tethyan Himalaya Series. These rocks are now located ~700 km from their easternmost outcrop in S-Tibet and ~450 km from Himalayan rocks in the Eastern Himalayan Syntaxis (EHS)—the northeastern edge of India. They record a high pressure-low temperature oceanic subduction-continental collision tectonic setting from ~65 to 30 Ma, formed at the northern front of India. They moved around the EHS and were involved in the northward growth of the Sagaing transform-fault (SF) system. The SF system imbricated the Indian-affinity rocks, and the Burma microplate—part of the intra-Tethyan Incertus-arc system.

Key Points:

- Indian-affinity Tethyan Himalaya Series occur in central Myanmar, ~450 km south of the Himalayan rocks in the Eastern Himalayan Syntaxis
- A low temperature-high pressure subduction-early collision system was active at ~65 Ma, peaked at ~45 Ma, and ended at ~30 Ma
- The Sagaing transform fault reactivated the Indus-Yarlung suture, and imbricated the Indian rocks and the Burma microplate from ~30 Ma on

Supporting Information:

Supporting Information may be found in the online version of this article.

Correspondence to:

L. Ratschbacher,
lothar@geo.tu-freiberg.de

Citation:

Min, M., Ratschbacher, L., Franz, L., Hacker, B. R., Enkelmann, E., Toreno, E. Y., et al. (2022). India (Tethyan Himalaya Series) in central Myanmar: Implications for the evolution of the Eastern Himalayan Syntaxis and the Sagaing transform-fault system. *Geophysical Research Letters*, *49*, e2022GL099140. https://doi.org/10.1029/2022GL099140

Received 12 APR 2022
Accepted 9 JUN 2022

Author Contributions:

Conceptualization: Myo Min, Lothar Ratschbacher, Birk Härtel, Bernd Schurr
Data curation: Myo Min, Lothar Ratschbacher, Leander Franz, Bradley R. Hacker, Eva Enkelmann
Formal analysis: Lothar Ratschbacher, Leander Franz, Bradley R. Hacker, Eva Enkelmann, Eko Yoan Toreno, Marion Tichomirowa, Jörg A. Pfänder
Funding acquisition: Lothar Ratschbacher, Bradley R. Hacker

1. Introduction

Indenter corners in collisional orogens—syntaxes—feature 3-D deformation with crustal thickening, lateral material flow, and transitions from continental to oceanic subduction. In the Cenozoic India-Asia collision zone, the underthrusting Indian craton has induced shortening in the Himalaya and Tibet, and lateral material flow out of the collision zone (e.g., Zhang et al., 2004; Zubovich et al., 2010). Pronounced lateral flow and clockwise vertical-axis rotations occur at and south of the Eastern Himalayan Syntaxis (EHS) where the Himalayan continental subduction transitions into the highly-oblique Burma oceanic subduction zone and the Sagaing transform-fault (SF) system (Figure 1a). Paleomagnetic studies in the Burma microplate, and the Asian-affinity Tengchong (Lhasa) and Baoshan (Qiangtang-Sibumasu) blocks indicate 40–90° clockwise, vertical-axis rotations in Myanmar and Yunnan since the Paleocene, changing the original ~W-strike of these blocks in Tibet to a ~N-strike south of the EHS (e.g., Kornfeld et al., 2014; Li et al., 2020, 2018; Westerweel et al., 2019).

Northward-widening cratonic India extends northeastward into the EHS region, and is rimmed in the east by the oceanic lithosphere of the Bay of Bengal. The current transition from continental collision to oceanic subduction must occur in the Indo-Burman Ranges (IBR), part of the Jurassic-Recent subduction-accretionary wedge that bounds the Indian plate in the east, because the footwall of the northern IBR is made up of the Indian continental crust of the Shillong Plateau (Figure 1a). The past position of this transition is unclear due to the intervening

Investigation: Myo Min, Lothar Ratschbacher, Leander Franz, Bradley R. Hacker, Eva Enkelmann, Eko Yoan Toreno
Methodology: Myo Min, Lothar Ratschbacher, Leander Franz, Bradley R. Hacker, Eva Enkelmann, Eko Yoan Toreno, Birk Härtel, Marion Tichomirowa, Jörg A. Pfänder
Project Administration: Lothar Ratschbacher, Bernd Schurr
Resources: Lothar Ratschbacher
Supervision: Lothar Ratschbacher
Validation: Myo Min, Lothar Ratschbacher, Leander Franz, Bradley R. Hacker, Bernd Schurr
Visualization: Myo Min, Lothar Ratschbacher
Writing – original draft: Myo Min, Lothar Ratschbacher
Writing – review & editing: Myo Min, Lothar Ratschbacher, Leander Franz, Bradley R. Hacker, Eva Enkelmann, Eko Yoan Toreno, Birk Härtel, Bernd Schurr, Marion Tichomirowa, Jörg A. Pfänder

Burma microplate and the northward-growing SF system, disrupting the Burma microplate, the IBR wedge, and the southern prolongation of the Indus-Yarlung suture (IYS) between India and Asia (e.g., Baxter et al., 2011).

To account for the ≥50 Ma onset of the India-Asia collision (e.g., Hu et al., 2016), a northern extension of cratonic India has been proposed. This Greater India is envisioned as a <2000-km-wide northward-projecting entity, consisting of extended continental and oceanic Indian lithosphere (e.g., van Hinsbergen et al., 2012) that has along its northern rim the Tethyan Himalaya Series (THS), on which the ophiolites of the IYS were emplaced.

Given that India's northward motion has been accommodated by subduction/shortening of Greater Indian and cratonic Indian lithosphere, lateral material flow out of the collision zone, and northward propagation of the Burma subduction zone and the SF system, tracing the evolution of the transition from continental collision to oceanic subduction, describing the initiation and evolution of the SF system, and reconstructing the eastern edge of Greater India are key aspects of understanding the India-Asia collision zone and of indenter corners in general. Here, we trace the eastern edge of India—represented by the THS—into central Myanmar. In the Katha Range, lithologic and provenance tracers and pressure-temperature-deformation-time (P-T-d-t) data outline a piece of the Cambro-Ordovician THS that experienced high-P–low-T metamorphism, exhumed rapidly in a subduction-early collisional tectonic setting, and was involved into the northward growth of the SF system. We show that the Katha rocks represent a distinct piece of subducted THS, similar only to the Lopu Range of central S-Tibet. These rocks allow the timing of the activity in the subduction-early collisional system and of the onset of strike-slip faulting along the SF system, and aid in the restauration of the eastern margin of India, in particular the SF system.

2. The Eastern Himalayan Syntaxis Region

Haproff et al. (2018, 2019, 2020) and Salvi et al. (2019) mapped the tectonostratigraphic units of India and Asia at the EHS (Dibang and Lohit valleys; Figure 1a), encountering the Asian Gangdese arc, the IYS (Tidding-Mayoda mélange), and the Indian Lesser Himalaya Series (LHS; Mayodia gneiss, Lalpani schist). The Greater Himalaya Series (GHS), THS (both India), and Xigaze forearc basin (Asia) are absent. Except for the Gangdese arc, none of the Himalayan–S-Tibet units have been traced unequivocally into the region south of the EHS (Figure 1a).

The ~NNE-trending Katha Range (Figure 1b) is bounded in the east by the 177–163 Ma (U-Pb zircon) Tagaung-Myitkyina suprasubduction-zone (ultra-)mafic rocks (Liu et al., 2016; Yang et al., 2012); they were intruded by (mostly) Cretaceous Gangdese-arc granitoids (Zhang et al., 2018). In the west, the Katha Range is bounded by the Namyin strand of the SF system. West of the Katha Range, rocks involved in the western strands of the SF include the Jurassic (Qiu et al., 2009; Shi et al., 2008) Jadeite belt, and various units of the Burma microplate and it cover—the Central Myanmar basin (Figures 1a and 1b). Sericite-chlorite-biotite-garnet schist, locally with amphibole, talc, and kyanite, quartzite, and marble have been reported from the Katha Range; their stratigraphic age may cover the early Paleozoic to Triassic (e.g., Mitchell, 2018; Zhang et al., 2018).

3. Katha Range: Lithology, Pressure-Temperature-Deformation-Time Evolution

Lithologically, we encountered porphyroblastic chloritoid-garnet-graphite micaschist, chlorite-chloritoid-bearing white-mica quartzite, and porphyroblastic staurolite-kyanite-garnet quartz micaschist. Locally, the Katha schists and quartzites enclose meter-thick meta-acidite tectonites, dominated by phengite and porphyric quartz, interpreted as volcanic layers or small hypabyssal intrusions. We used zircon and rutile U-Pb geochronology to determine (a) the igneous emplacement ages and (b) the maximum deposition age and (c) provenance of the meta-sedimentary rocks to establish correlations with rocks of the Himalaya and S-Tibet. The sample petrography, the geo-thermochronologic methods, their results, and the analytical data are provided in the Texts S1 and S2 of Supporting Information S1, Tables S1 and S2, and in Min et al. (2022).

Two meta-acidites yielded U-Pb zircon crystallization ages of 501 ± 9 and 530 ± 5 Ma (2s; Figure S1 in Supporting Information S1 and Min et al., 2022); both samples contain a large number of inherited (older) zircons. Figure 2a compares the inherited (meta-acidites) and detrital (meta-sedimentary rocks) U-Pb zircon and rutile ages: the zircon age distributions of all samples are similar, with clusters at ~500 and 1,000 Ma; nearly all detrital rutile ages are at ~500 Ma. The youngest detrital zircon and rutile grains are 482 + 7/–19 and 463 + 8/–10 Ma, respectively (calculated with the "Youngest Zircon" routine and "third degree of youngest option," Isoplot4.5; Ludwig, 2008). These dates suggest a Cambro-Ordovician age for the studied Katha rocks.

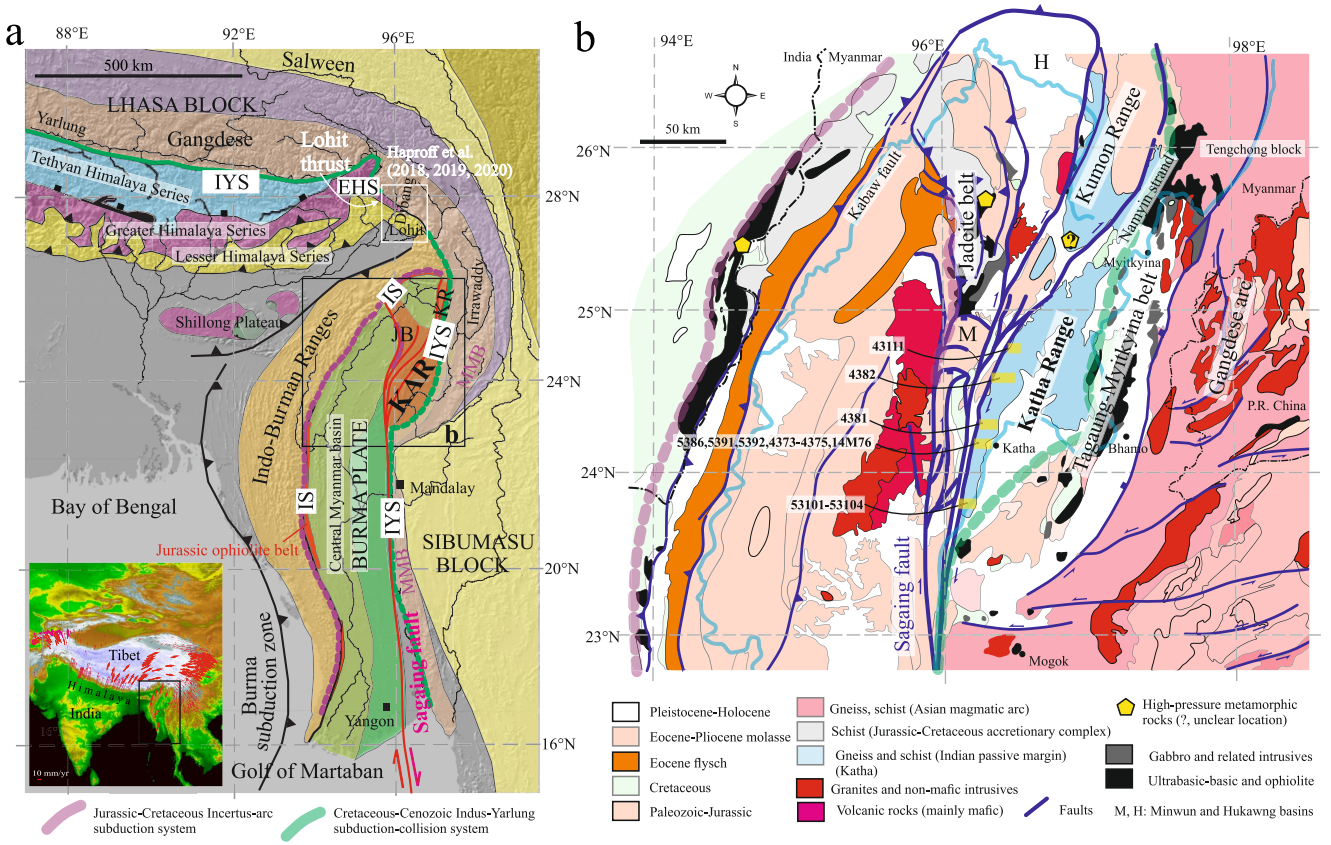

Figure 1. (a) Eastern Himalayan Syntaxis and eastern margin of the Indian plate (modified from Robinson et al., 2014). The Burma microplate—colored green—is rimmed by the Incertus-arc and Indus-Yarlung sutures; it is partly covered by the Central Myanmar basin. The Incertus-arc suture was south (in the Cretaceous) of the Incertus arc, defined by Westerweel et al. (2019); this arc was part of the Trans-Tethyan subduction system of Hall (2012). Insert locates (a) and shows Eurasia-fixed GNSS-derived displacement field. (b) Geological map centered on the Katha Range modified from Geological Map of Myanmar (2014) and Wang and Burchfiel (1997). Sagaing transform-fault system modified from Morley and Arboit (2019) and Maurin et al. (2010). Yellow bars: studied traverses and samples (see Text S1 in Supporting Information S1 and Table S1 for detailed sample location). EHS, Eastern Himalayan Syntaxis; IYS, Indus-Yarlung Suture; IS, Incertus-arc suture (Jurassic-Cretaceous ophiolite belt); JB, Jadeite Belt; KAR, Katha Range; KR, Kumon Range; MMB, Mogok Metamorphic Belt; TMB, Tagaung-Myitkyina Belt.

Figure 3a plots the Katha-rock P-T data together with THS data from central S-Tibet (Laskowski et al., 2016), eastern S-Tibet (Dunkl et al., 2011; Fang et al., 2020), and GHS and LHS data from Bhutan (Daniel et al., 2003). The P-T results are summarized in Supporting Information Table S4, and the petrology—derived from THERIAK/DOMINO equilibrium-assemblage calculations and conventional thermobarometry—is detailed in Text S1 of Supporting Information S1 and Min et al. (2022). Four meta-sedimentary rocks yielded prograde P-T data of 470–510°C, 1.0–1.5 GPa and peak data at 490–551°C, 0.8–1.0 GPa; one sample has higher temperatures (prograde ~535°C, 1.0 GPa, peak ~650°C, 1.0 GPa). Figure 3b plots the Katha-rock T-t history. The meta-acidite zircon ages, the youngest detrital zircon age groups, and the detrital rutile ages (all U-Pb) indicate a Cambro-Ordovician intrusion (zircon) and cooling (rutile) event. U-Pb monazite and rutile, Rb-Sr phengite, $^{40}Ar/^{39}Ar$ phengite and biotite, zircon (ZFT) and apatite (AFT) fission track, and zircon (U-Th)/He (ZHe) dates outline the Cenozoic evolution. We calculated closure-temperatures, T_c, with CLOSURE (Brandon et al., 1998). For Ar/Ar phengite, we used a T_c of ~450°C, accounting for slower diffusional loss at elevated pressures (e.g., Harrison et al., 2009; Warren et al., 2012). Changes in the actual T_c have little effect on the T-t history.

Given a ~550°C T_c for the Rb-Sr phengite system (e.g., Blanckenburg et al., 1989)—higher than the average peak-T (~510°C)—the two dates ≥55 Ma likely are formation ages during prograde metamorphism (~483°C average T). The same may apply for the U-Pb rutile date (~50 Ma; T_c of 500–650°C; e.g., Kooijman et al., 2010; Ewing et al., 2015) of quartzite 53101A, whose 500–800°C T-range from Zr-in-rutile isopleths (Figure S1 in Supporting Information S1) indicates incomplete reset of detrital rutile. The 500–550°C Zr-in-rutile-derived T-range of 44–36 Ma rutiles indicates metamorphic growth in meta-acidite 5386A, distinctly different from

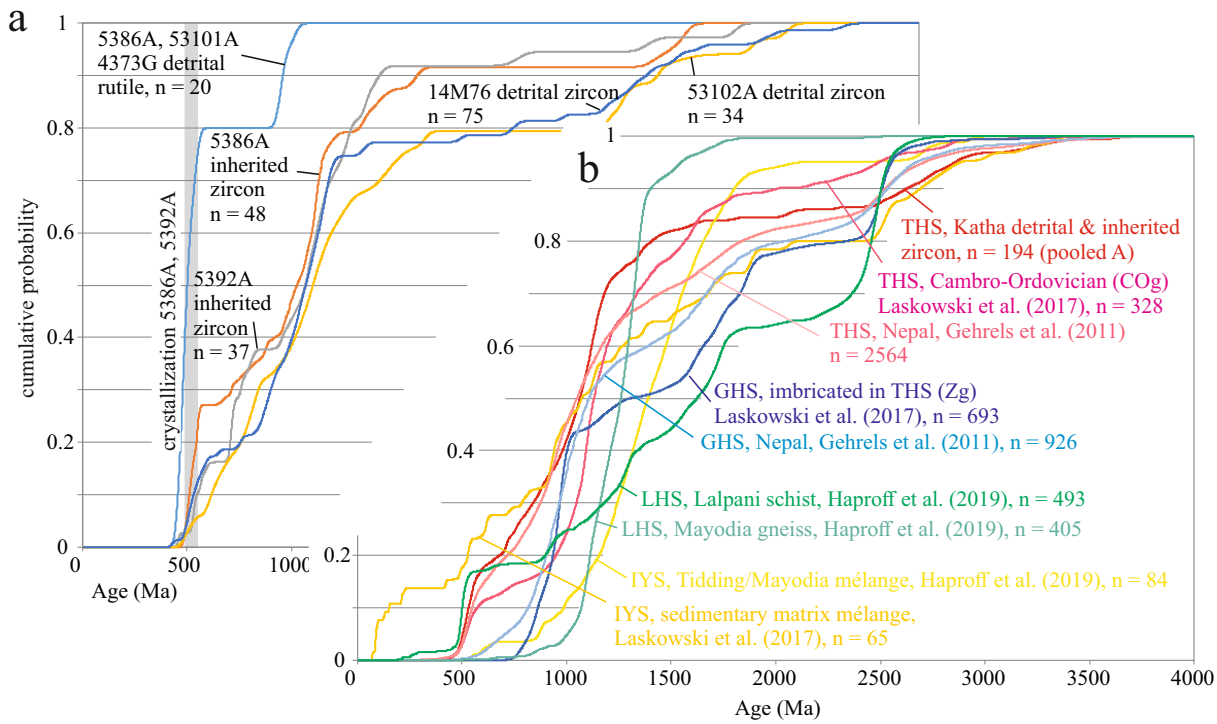

Figure 2. Cumulative probability plots of U-Pb zircon and rutile ages of (a) samples from this study and sample 14M76 of Zhang et al. (2018), and (b) their comparison with rocks from central and eastern S-Tibet and the central and eastern Himalaya. Ages used include 2s uncertainties and have 90–110% $^{206}Pb/^{238}U$–$^{207}Pb/^{206}Pb$ age concordance. THS, Tethyan Himalaya Series; GHS, Greater Himalaya Series; LHS, Lesser Himalaya Series; IYS, Indus-Yarlung Suture.

the higher-T of inherited grains (Figure S1 in Supporting Information S1). Peak-T is likely best dated by the 48–42 Ma monazite inclusions (~10 μm) in poikiloblastic kyanite of sample 4382. Taken together, the T-t path comprises prograde metamorphism from ~65 Ma to peak P-T at ~45 Ma (~55 km burial, assuming a lithostatic gradient of ~37 km/GPa), cooling at ~25°C/Myr to ~30 Ma, and cooling at ~4°C/Myr thereafter (Figure 3b).

Figure 3c compiles structural data of the Katha rocks along two traverses. Bedding (s_0) and foliation (s_1) occupy a great-circle distribution, recording open to tight folds with ~NNW-trending axes (B_2), subparallel to mineral stretching lineation str_1. S_1 and str_1 are associated with folded shear zones/bands that indicate ~NNW-SSE stretch with dominant top-to-SSE shear, also indicated by sigma clasts and asymmetric foliation boudinage (c.f., Passchier & Trouw, 2005). Overprinting a relict fabric, s_1, str_1, and the shear fabrics are outlined by the syn- to post-peak P-T mineral assemblage; they likely record exhumation by crustal extension. The folds record the regional ~E-W shortening south of the EHS (e.g., Wang & Burchfiel, 1997).

4. Discussion

We focus on four salient questions: What Himalaya-Tibet series do the Katha rocks represent? How and when were they exhumed? Which position did they occupy in the evolution of the India-Asia collision system? When and how were they involved in the oblique plate boundary south of the EHS, in particular the SF system?

Lithologically, the Katha rocks are part of the THS and most similar to the Cambro-Ordovician gneiss-schist unit in central S-Tibet (Lopu Range; Laskowski et al., 2017). Figure 2b compares the inherited and detrital zircon ages of the Katha rocks with possibly equivalent tectonostratigraphic units in the Himalaya and S-Tibet, that is, the Cambro-Ordovician THS of the Lopu Range of central S-Tibet, the Nepal THS, the central Himalaya and Nepal GHS, the LHS units at the EHS, the IYS in the central Himalaya and at the EHS (Gehrels et al., 2011; Haproff et al., 2019; Laskowski et al., 2016); we chose these units because of their proximity to the EHS, similar P-T-d-t history (central S-Tibet), and large database (Nepal). The Katha rocks compare best to the THS, and least to the IYS, LHS, and GHS rocks.

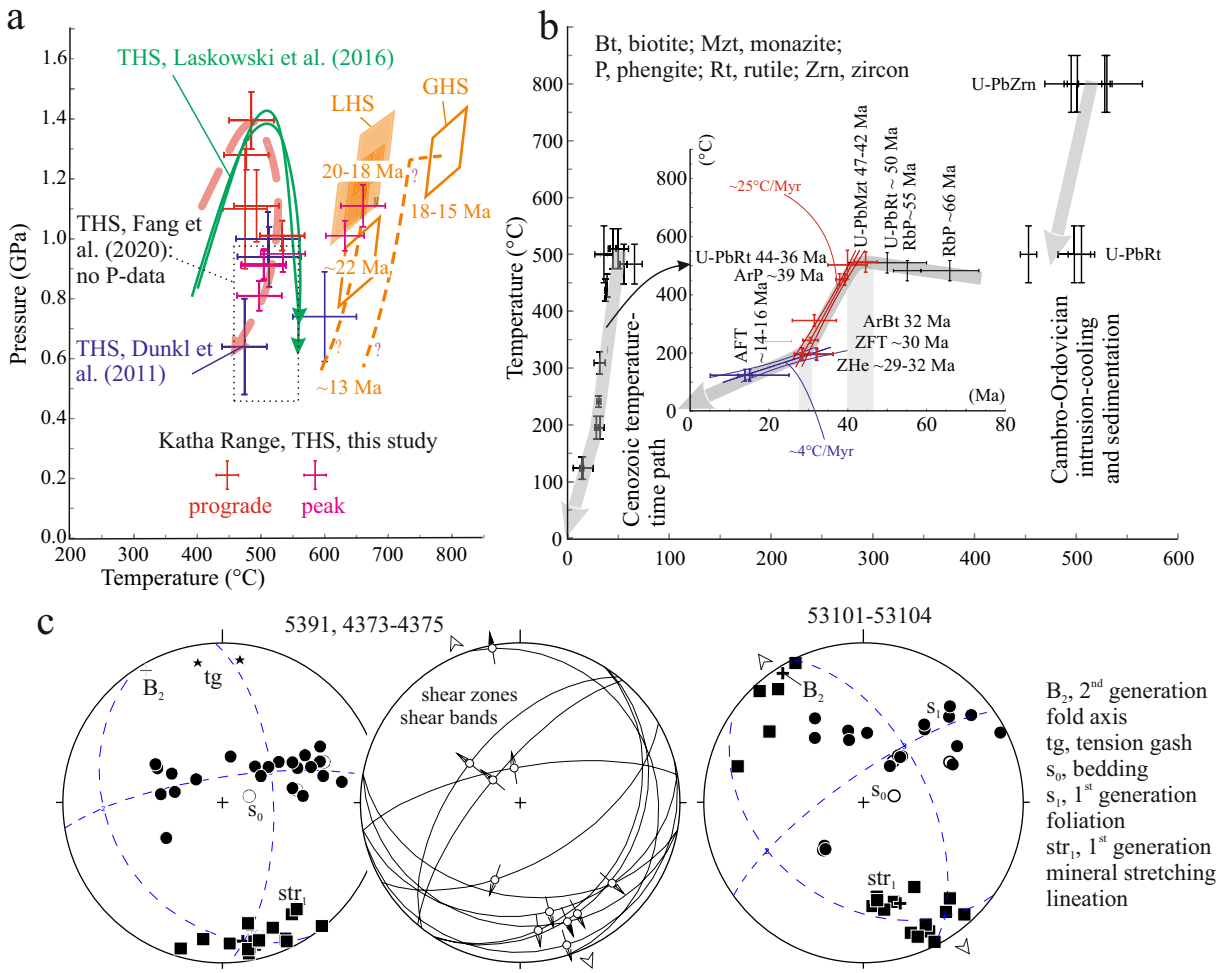

Figure 3. Pressure-temperature-time-deformation (P-T-t-d) data. (a) P-T of the Katha rocks and comparison with data from central and eastern S-Tibet and the eastern Himalaya. Our new prograde and peak data are 470–510°C, 1.0–1.5 GPa, reached at >65–45 Ma, and 490–551°C, 0.8–1.0 GPa, reached at ~45 Ma, respectively. The data from the Greater Himalaya Series (GHS) and Lesser Himalaya Series (LHS) are from Bhutan (Daniel et al., 2003). (b) T-t paths, and (c) structural data of the Katha rocks; see Figure 1b for traverses studied and Text S1 in Supporting Information S1 for detailed location of samples. THS, Tethyan Himalaya Series.

Petrologically, the Katha-rock data (Figure 3a; red P-T path) are most similar to the THS data of central S-Tibet (Figure 3a; green P-T paths; Laskowski et al., 2016); there, metamorphism at ≥1.4 GPa, ≤600°C peaked at ~40 Ma and the rocks cooled rapidly through 39–34 Ma. These P-T data—our new and those of Laskowski et al. (2016)—represent dramatic/highest conditions, different for the bulk of the THS, which record lesser conditions. These high-P/low-T conditions likely record local involvement of THS rocks into the subduction channel. In eastern S-Tibet, the basal THS rocks experienced comparable-T but lower-P (~600°C, 0.78 GPa; Dunkl et al., 2011; 510 ± 50°C, Fang et al., 2020; Figure 3a), and similar burial-early exhumation histories like those inferred for Katha (~49–32 Ma; U-Pb zircon, K(Ar)/Ar mica; for example, Aikman et al., 2008, 2012; Dunkl et al., 2011; Ratschbacher et al., 1994). In the same area of eastern S-Tibet, post-thrusting uppermost GHS granitoids have 48–36 Ma U-Pb zircon ages; the associated schists show higher-T and lower-P (~630–660°C, 0.7–0.8 GPa; Ding, Zhang, Dong, et al., 2016; Ding, Zhang, Hu, et al., 2016) than the Katha rocks. Different from the latter, both the THS and GHS rocks experienced Miocene heating and rapid cooling (~18–12 Ma; e.g., Aikman et al., 2008, 2012; Ding, Zhang, Hu, et al., 2016; Dunkl et al., 2011). The IYS rocks of the southern EHS (Tidding-Mayodia mélange) record metamorphism and ~30°C/Myr cooling between 40 and 30 Ma and rapid Miocene cooling (~11–6 Ma; ZHe ages; Haproff et al., 2020), not documented in the Katha rocks. The Katha P-T-t data contrast with GHS and

LHS data in Bhutan (Figure 3a; e.g., Daniel et al., 2003). Lithology and P-T-t evolution are compatible with the Katha rocks being a piece of the basal—Cambro-Ordovician—THS, now located ~700 km southeast of the last exposure of the THS in eastern S-Tibet, and ~450 km south of the Himalayan rocks in the Lohit valley at the southern edge of the EHS.

Structural studies in eastern S-Tibet outlined top-to-S thrusts and S-facing folds, overprinted by N-facing folds close to the Great Counter Thrust along the IYS (e.g., Dunkl et al., 2011; Ratschbacher et al., 1994). Detachments—most with top-to-N kinematics—separate the GHS and THS and occur within the basal THS (e.g., Ding, Zhang, Dong, et al., 2016; Ding, Zhang, Hu, et al., 2016). In the southern EHS, Haproff et al. (2018) mapped thrusts with a ≤90° clockwise change in displacement directions. The Katha rocks preserve—besides relict deformation—fabrics akin to the detachments in the THS. Assuming 60–90° clockwise rotation due to the motion of the Indian-affinity (THS of Katha) and Asian-affinity (Tengchong–Gangdese) rocks of central and eastern Myanmar and Yunnan around the EHS, the top-to-SSE flow in the Katha THS rocks restores to top-to- ~E flow, deflected ~90° from the typical top-to-N flow in S-Tibet. The younger, ~NNW-trending folds parallel the present-day structural grain and appear unrotated.

Whereas the exhumation history is similar to the basal section of the THS in the Lopu Range of central S-Tibet, and on a first order comparable to some THS localities in eastern S-Tibet, two aspects of the Katha rocks stand out: the lack of a Miocene heating and rapid cooling event and the top-to-~E normal-sense exhumation. We attribute the ~45–30 Ma rapid cooling from a high-P/low-T peak as due to exhumation from ~55-km-depth in a subduction-early collision tectonic setting at the leading edge of Greater India, as also observed in the THS rocks of the Lopu Range of central S-Tibet (Laskowski et al., 2016); however, the peak metamorphism and onset of exhumation occurred ~5 Myr earlier in the Katha Range. The top-to-~E exhumation kinematics may indicate that the Katha rocks were positioned at the easternmost end of the Himalaya.

The initiation of the SF system has been bracketed to middle Miocene-early Pliocene, based on the onset of seafloor spreading in the Andaman rift (e.g., Bertrand & Rangin, 2003). Morley and Arboit (2019) proposed a 28–27 Ma onset, based on the age of the basal strata in a releasing-bend basin (Minwun basin, Figure 1b) along a SF strand in northern Myanmar. The change from ~25 to ~4°C/Myr cooling of the Katha rocks at ~30 Ma may signify their involvement into the SF system, when it started to interact with the THS thrust-fold belt that acquired a ~N-strike during the northward propagation of India's eastern tip. The movement around the EHS also allowed the Katha rocks to escape the intense shortening at the collision front, thus a Miocene overprint.

Figure 4 summarizes our proposed evolution of the EHS and the SF system: At ~60 Ma (Figure 4a), the intra-Tethyan Incertus-arc system—which the Burma microplate was part of—terminated (Westerweel et al., 2019). The highly-oblique plate boundary along Greater India's eastern margin offset the Burma microplate (at ~5°N) from the leading Greater India subduction in the north; collision with the Indian margin rotated it ~40° clockwise (~60–40 Ma; Li et al., 2020). Continental subduction may have started at ≥47 Ma at both syntaxes, as indicated in the western Himalaya (Tso Morari; Donaldson et al., 2013) and the Katha range. The IYS at the eastern edge of the Burma microplate was reactivated as the SF system (Figure 4b); the ~30 Ma initiation of the SF system terminated the Katha-rock cooling/exhumation in the subduction-collision tectonic setting and initiated the transition to strike-slip motion with a much-reduced cooling/exhumation rate. The SF system connected with the THS thrust-fold belt at the EHS, where the THS were later subducted together with the GHS (Haproff et al., 2020).

Figures 4c and 4d show the evolution of the SF system: the eastern Namyin strand allows restoration of the Jadeite belt and the northernmost section of the Jurassic ophiolite belt (Incertus suture) to the south, at least to the southern tip of the Indian rocks—south of the Katha Range; a western strand and the Kabaw fault allow the restoration of the central and southern Jurassic ophiolite belt, connecting it to the south of the Jadeite belt. The entire area south of the EHS—including the SF system—experienced further clockwise rotation and ~E-W shortening—recorded by folding-thrusting (our data; Maurin & Rangin, 2009) and geodetic data (e.g., Maurin et al., 2010)—during the evolution of the Burma subduction system and the collision of the northward-moving Burma microplate with the Shillong plateau.

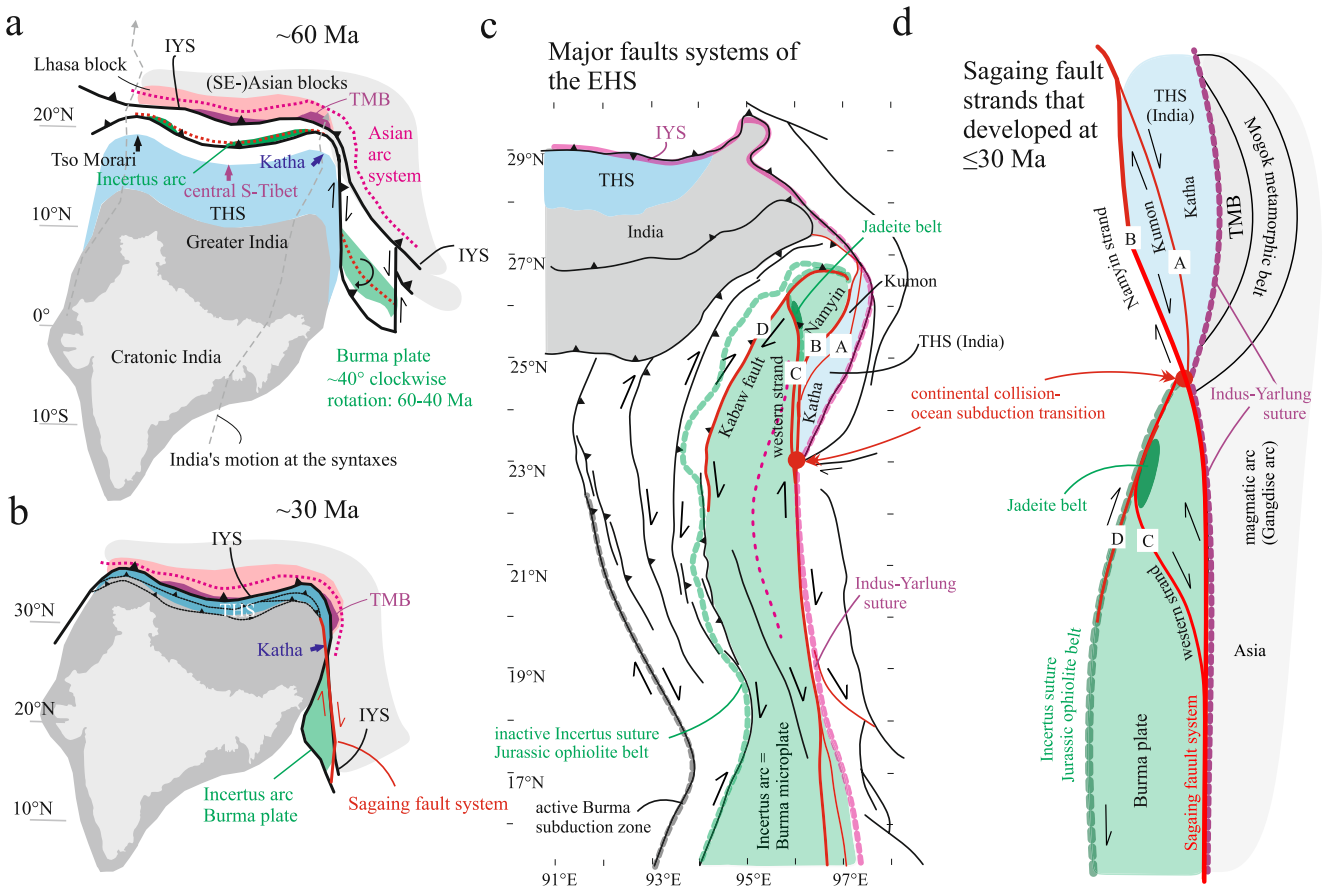

Figure 4. The Katha Range in the evolution of the Eastern Himalayan Syntaxis (EHS) and the Sagaing transform-fault system (SF). The nomenclature "Incertus arc" follows Westerweel et al. (2019), and describes the island-arc system of the Trans-Tethyan subduction system of Hall (2012). (a) Incipient Himalaya-Tibet formation following Incertus-arc subduction with the Burma microplate at the arc's eastern end. (b) Development of the SF system along the Indus-Yarlung suture (IYS) and its connection with the Tethyan Himalaya Series (THS) fold-thrust belt. (c) Major fault systems of the EHS. (d) Restoration of the imbrication of the Incertus-arc subduction system at the western margin of the Burma microplate. Growth of the SF system imbricated the northern part of the Burma microplate, isolated the Jadeite belt and the northernmost part of the Jurassic ophiolite belt, and imbricated the Indian rocks of the Katha and Kumon Ranges. A to D demark major strands of the SF system and do not imply a time sequence of formation. Abbreviations: IYS, Indus-Yarlung Suture; THS, Tethyan Himalaya Series; TMB, Tagaung-Myitkyina Belt.

Conflict of Interest

The authors declare no conflicts of interest relevant to this study.

Data Availability Statement

The petrologic and geo-thermochronologic data are available as Supporting Information S1 in the online version of this article and (CC-BY 4.0 license) and are available through GFZ data services (https://doi.org/10.5880/fidgeo.2022.025; Min et al., 2022).

Acknowledgments
Funded by DFG RA 442/28. We acknowledge reviews by A.A.G. Webb and an anonymous colleague and editorial handing by L. Flesch. Open Access funding enabled and organized by Projekt DEAL.

References

Aikman, A. B., Harrison, T. M., & Ding, L. (2008). Evidence for early (>44 Ma) crustal thickening, Tethyan Himalaya, southeastern Tibet. *Earth and Planetary Science Letters*, *274*, 14–23. https://doi.org/10.1016/j.epsl.2008.06.038

Aikman, A. B., Harrison, T. M., & Hermann, J. (2012). Age and thermal history of Eo- and Neohimalayan granitoids, eastern Himalaya. *Journal of Asian Earth Sciences*, *51*, 85–97. https://doi.org/10.1016/j.jseaes.2012.01.011

Baxter, A. T., Aitchison, J. C., Zyabrev, S. V., & Ali, J. R. (2011). Upper Jurassic radiolarites from the Naga ophiolite, Nagaland, northeast India. *Gondwana Research*, *20*, 638–644. https://doi.org/10.1016/j.gr.2011.02.001

Bertrand, G., & Rangin, C. (2003). Tectonics of the western margin of the Shan Plateau (central Myanmar): Implication for the India-Indochina oblique convergence since the Oligocene. *Journal of Asian Earth Sciences*, *21*, 1139–1157. https://doi.org/10.1016/s1367-9120(02)00183-9

Blanckenburg, v. F., Villa, I. M., Baur, H., Morteani, G., & Steiger, R. H. (1989). Time calibration of a PT-path from the Western Tauern Window, Eastern Alps: The problem of closure temperatures. *Contributions to Mineralogy and Petrology*, *101*, 1–11. https://doi.org/10.1007/bf00387196

Brandon, M. T., Roden-Tice, M. K., & Garver, J. I. (1998). Late Cenozoic exhumation of the Cascadia accretionary wedge in the Olympic Mountains, northwest Washington State. *The Geological Society of America Bulletin*, *110*, 985–1009. https://doi.org/10.1130/0016-7606(1998)110<0985:lceotc>2.3.co;2

Daniel, C. G., Hollister, L. S., Parrish, R. R., & Grujic, D. (2003). Exhumation of the Main Central Thrust from lower crustal depths, eastern Bhutan Himalaya. *Journal of Metamorphic Geology*, *21*, 317–334. https://doi.org/10.1046/j.1525-1314.2003.00445.x

Ding, H., Zhang, Z., Dong, X., Tan, Z., Xiang, H., Mu, H., et al. (2016). Early Eocene (*c*. 50Ma) collision of the Indian and Asian continents: Constraints from the North Himalayan metamorphic rocks, southeastern Tibet. *Earth and Planetary Science Letters*, *435*, 64–73. https://doi.org/10.1016/j.epsl.2015.12.006

Ding, H., Zhang, Z., Hu, K., Dong, X., Xiang, H., & Mu, H. (2016). P-T-t-D paths of the North Himalayan metamorphic rocks: Implications for the Himalayan orogeny. *Tectonophysics*, *683*, 393–404. https://doi.org/10.1016/j.tecto.2016.06.035

Donaldson, D. G., Webb, A. A. G., Menold, C. A., Kylander-Clark, A. R. C., & Hacker, B. R. (2013). Petrochronology of Himalayan ultrahigh-pressure eclogite. *Geology*, *41*, 835–838. https://doi.org/10.1130/g33699.1

Dunkl, I., Antolín, B., Wemmer, K., Rantitsch, G., Kienast, M., Montomoli, C., et al. (2011). Metamorphic evolution of the Tethyan Himalayan flysch in SE Tibet. *Geological Society - Special Publications*, *353*, 45–69. https://doi.org/10.1144/sp353.4

Ewing, T. A., Rubatto, D., Beltrando, M., & Hermann, J. (2015). Constraints on the thermal evolution of the Adriatic margin during Jurassic continental break-up: U–Pb dating of rutile from the Ivrea–Verbano Zone, Italy. *Contributions to Mineralogy and Petrology*, *169*, 44. https://doi.org/10.1007/s00410-015-1135-6

Fang, D.-R., Zhang, J., Hisada, K.-I., Wang, G.-H., & Li, D. (2020). Geological anatomy of the Upper Triassic sequence in southeastern Tibet: Implications for tectonic evolution of the eastern Himalayan Orogen. *Geological Journal*, *55*, 6607–6624. https://doi.org/10.1002/gj.3831

Gehrels, G., Kapp, P., DeCelles, P., Pullen, A., Blakey, R., Weislogel, A., et al. (2011). Detrital zircon geochronology of pre-Tertiary strata in the Tibetan-Himalayan orogen. *Tectonics*, *30*. https://doi.org/10.1029/2011TC002868

Geological Map of Myanmar (2014). *Geological Map of Myanmar* (pp. 1–32). Myanmar Geosciences Society.

Hall, R. (2012). Late Jurassic–Cenozoic reconstructions of the Indonesian region and the Indian Ocean. *Tectonophysics*, *570–571*, 1–41. https://doi.org/10.1016/j.tecto.2012.04.021

Haproff, P. J., Odlum, M. L., Zuza, A. V., Yin, A., & Stockli, D. F. (2020). Structural and thermochronologic constraints on the Cenozoic tectonic development of the northern Indo-Burma Ranges. *Tectonics*, *39*(9), e2020TC006231. https://doi.org/10.1029/2020TC006231

Haproff, P. J., Zuza, A. V., & Yin, A. (2018). West-directed thrusting south of the eastern Himalayan syntaxis indicates clockwise crustal flow at the indenter corner during the India-Asia collision. *Tectonophysics*, *722*, 277–285. https://doi.org/10.1016/j.tecto.2017.11.001

Haproff, P. J., Zuza, A. V., Yin, A., Harrison, T. M., Manning, C. M., Ding, L., et al. (2019). Geologic framework of the northern Indo-Burma Ranges: Lateral correlation of Himalayan-Tibetan lithologic units across the eastern Himalayan syntaxis. *Geosphere*, *15*, 856–881.

Harrison, T. M., Célérier, J., Aikman, A. B., Hermann, J., & Heizler, M. T. (2009). Diffusion of ^{40}Ar in muscovite. *Geochimica et Cosmochimica Acta*, *73*, 1039–1051. https://doi.org/10.1016/j.gca.2008.09.038

Hu, X., Garzanti, E., Wang, J., Huang, W., & Webb, A. A. G. (2016). The timing of India–Asia collision onset – Facts, theories, controversies. *Earth-Science Reviews*, *160*, 264–299. https://doi.org/10.1016/j.earscirev.2016.07.014

Kooijman, E., Mezger, K., & Berndt, J. (2010). Constraints on the U–Pb systematics of metamorphic rutile from in situ LA ICP-MS analysis. *Earth and Planetary Science Letters*, *293*, 321–330. https://doi.org/10.1016/j.epsl.2010.02.047

Kornfeld, D., Eckert, S., Appel, E., Ratschbacher, L., Sonntag, B. L., Pfänder, J. A., et al. (2014). Cenozoic clockwise rotation of the Tengchong block, southeastern Tibetan Plateau: A paleomagnetic and geochronologic study. *Tectonophysics*, *628*, 105–122. https://doi.org/10.1016/j.tecto.2014.04.032

Laskowski, A. K., Kapp, P., Ding, L., Campbell, C., & Liu, X. H. (2017). Tectonic evolution of the Yarlung suture zone, Lopu Range region, southern Tibet. *Tectonics*, *36*, 108–136. https://doi.org/10.1002/2016tc004334

Laskowski, A. K., Kapp, P., Vervoort, J. D., & Ding, L. (2016). High-pressure Tethyan Himalaya rocks along the India-Asia suture zone in southern Tibet. *Lithosphere*, *8*, 574–582. https://doi.org/10.1130/l544.1

Li, S., van Hinsbergen, D. J. J., Deng, C., Advokaat, E. L., & Zhu, R. (2018). Paleomagnetic constraints from the Baoshan area on the deformation of the Qiangtang-Sibumasu terrane around the eastern Himalayan syntaxis. *Journal of Geophysical Research: Solid Earth*, (2), 977. https://doi.org/10.1002/2017jb015112

Li, Z., Ding, L., Zaw, T., Wang, H., Cai, F., Yao, W., et al. (2020). Kinematic evolution of the West Burma block during and after India-Asia collision revealed by paleomagnetism. *Journal of Geodynamics*, *134*, 101690. https://doi.org/10.1016/j.jog.2019.101690

Liu, C.-Z., Chung, S.-L., Wu, F.-Y., Zhang, C., Xu, Y., Wang, J.-G., et al. (2016). Tethyan suturing in Southeast Asia: Zircon U-Pb and Hf-O isotopic constraints from Myanmar ophiolites. *Geology*, *44*, 311–314. https://doi.org/10.1130/g37342.1

Ludwig, K. (2008). *User's Manual for Isoplot4.5* (Vol. 4, pp. 1–75). Berkeley Geochronology Center Special Publication.

Maurin, T., Masson, F., Rangin, C., Min, U. T., & Collard, P. (2010). First global positioning system results in northern Myanmar: Constant and localized slip rate along the Sagaing fault. *Geology*, *38*, 591–594. https://doi.org/10.1130/g30872.1

Maurin, T., & Rangin, C. (2009). Structure and kinematics of the Indo-Burmese wedge: Recent and fast growth of the outer wedge. *Tectonics*, *28*, TC2010. https://doi.org/10.1029/2008TC002276

Min, M., Ratschbacher, L., Franz, L., Hacker, B. R., Enkelmann, E., Toreno, E. Y., et al. (2022). *Provenance and pressure-temperature-time-deformation evolution of Indian crust in central Myanmar*. GFZ Data Services. https://doi.org/10.5880/fidgeo.2022.025

Mitchell, A. (2018). *Geological belts, plate boundaries, and Mineral deposits in Myanmar* (p. 524). Elsevier.

Morley, C. K., & Arboit, F. (2019). Dating the onset of motion on the Sagaing fault: Evidence from detrital zircon and titanite U-Pb geochronology from the North Minwun Basin, Myanmar. *Geology*, *47*, 581–585. https://doi.org/10.1130/g46321.1

Passchier, C. W., & Trouw, R. A. J. (2005). *Microtectonics* (p. 1). Springer Verlag.

Qiu, Z., Wu, F.-Y., Yang, S.-F., Zhu, M., Sun, J.-F., & Yang, P. (2009). Age and genesis of the Myanmar jadeite: Constraints from U-Pb ages and Hf isotopes of zircon inclusions. *Chinese Science Bulletin*, *54*, 658–668. https://doi.org/10.1007/s11434-008-0490-3

Ratschbacher, L., Frisch, W., Liu, G., & Chen, C. C. (1994). Distributed deformation in southern and western Tibet during and after the India–Asia collision. *Journal of Geophysical Research*, *99*, 19917–19945. https://doi.org/10.1029/94jb00932

Robinson, R. A. J., Brezina, C. A., Parrish, R. R., Horstwood, M. S. A., Oo, N. W., Bird, M. I., et al. (2014). Large rivers and orogens: The evolution of the Yarlung Tsangpo–Irrawaddy system and the eastern Himalayan syntaxis. *Gondwana Research*, *26*, 112–121. https://doi.org/10.1016/j.gr.2013.07.002

Salvi, D., Mathew, G., Kohn, B., Pande, K., & Borgohain, B. (2019). Thermochronological insights into the morphotectonic evolution of Mishmi hills across the Dibang Valley, NE Himalayan Syntaxis. *Journal of Asian Earth Sciences*, *190*, 104158. https://doi.org/10.1016/j.jseaes.2019.104158

Shi, G., Cui, W., Cao, S., Jian, N., Jian, P., Liu, D., et al. (2008). Ion microprobe zircon U-Pb age and geochemistry of the Myanmar jadeitite. *Journal Geological Society of London*, *165*, 221–234. https://doi.org/10.1144/0016-76492006-119

Van Hinsbergen, D. J. J., Lippert, P. C., Dupont-Nivet, G., McQuarrie, N., Doubrovine, P. V., Spakman, W., & Torsvik, T. H. (2012). Greater India basin hypothesis and a two-stage Cenozoic collision between India and Asia. *Proceedings of the National Academy of Sciences*, *109*, 7659–7664. https://doi.org/10.1073/pnas.1117262109

Wang, E., & Burchfiel, B. C. (1997). Interpretation of Cenozoic tectonics in the right-lateral accommodation zone between the Aialo Shan shear zone and the Eastern Himalayan Syntaxis. *International Geological Review*, *39*, 191–219. https://doi.org/10.1080/00206819709465267

Warren, C. J., Hanke, F., & Kelley, S. P. (2012). When can muscovite $^{40}Ar/^{39}Ar$ dating constrain the timing of metamorphic exhumation? *Chemical Geology*, *291*, 79–86. https://doi.org/10.1016/j.chemgeo.2011.09.017

Westerweel, J., Roperch, P., Licht, A., Dupont-Nivet, G., Win, Z., Poblete, F., et al. (2019). Burma terrane part of the Trans-Tethyan arc during collision with India according to paleomagnetic data. *Nature Geoscience*, *12*, 863–868. https://doi.org/10.1038/s41561-019-0443-2

Yang, J. S., Xu, Z. Q., Duan, X. D., Xiong, F. H., Liu, Z., Cai, Z. H., & Li, H. Q. (2012). Discovery of a Jurassic SSZ ophiolite in the Myitkyina region of Myanmar. *Acta Petrologica Sinica*, *28*, 1710–1730.

Zhang, J., Xiao, W., Windley, B. F., Wakabayashi, J., Cai, F., Seing, K., et al. (2018). Multiple alternating forearc- and backarc-ward migration of magmatism in the Indo-Myanmar Orogenic Belt since the Jurassic: Documentation of the orogenic architecture of eastern Neotethys in SE Asia. *Earth-Science Reviews*, *185*, 704–731. https://doi.org/10.1016/j.earscirev.2018.07.009

Zhang, P. Z., Shen, Z., Wang, M., Gan, W., Bürgmann, R., Molnar, P., et al. (2004). Continuous deformation of the Tibetan Plateau from global positioning system data. *Geology*, *32*, 809–812. https://doi.org/10.1130/g20554.1

Zubovich, A. V., Wang, X. Q., Scherba, Y. G., Schelochkov, G. G., Reilinger, R., Reigber, C., et al. (2010). GPS velocity field of the Tien Shan and surrounding regions. *Tectonics*, *29*, TC6014. https://doi.org/10.1029/2010TC002772

References From the Supporting Information

Bohlen, S. R., & Liotta, J. J. (1986). A barometer for garnet amphiboles and garnet granulites. *Journal of Petrology*, *27*, 1025–1034. https://doi.org/10.1093/petrology/27.5.1025

De Capitani, C. (1994). Gleichgewichts-Phasendiagramme: Theorie und Software. *Beihefte zum European Journal of Mineralogy*, *1*(6), 48.

Farley, K. A., Wolf, R. A., & Silver, L. T. (1996). The effects of long alpha-stopping distances on (U-Th)/He dates. *Geochimica et Cosmochimica Acta*, *60*, 4223–4230. https://doi.org/10.1016/s0016-7037(96)00193-7

Frei, D., & Gerdes, A. (2009). Precise and accurate in situ U-Pb dating of zircon with high sample throughput by automated LA-SF-ICP-MS. *Chemical Geology*, *261*, 261–270. https://doi.org/10.1016/j.chemgeo.2008.07.025

Ghent, E. D., Stout, M. Z., Black, P. M., & Brothers, R. N. (1987). Chloritoid bearing rocks with blueschists and eclogites, northern New Caledonia. *Journal of Metamorphic Geology*, *5*, 239–254. https://doi.org/10.1111/j.1525-1314.1987.tb00382.x

Holdaway, M. J. (2000). Application of new experimental and garnet Margules data to the garnet-biotite geothermometer. *American Mineralogist*, *85*, 881–892. https://doi.org/10.2138/am-2000-0701

Hynes, A., & Forest, R. C. (1988). Empirical garnet-muscovite geothermometry in low-grade metapelites, Selwyn Range (Canadian Rockies). *Journal of Metamorphic Geology*, *6*, 297–309. https://doi.org/10.1111/j.1525-1314.1988.tb00422.x

Jarosewich, E., Nelen, J. A., & Norberg, J. A. (1980). Reference samples for electron microprobe analysis. *Geostandards Newsletter*, *4*, 43–47. https://doi.org/10.1111/j.1751-908x.1980.tb00273.x

Käßner, A., Ratschbacher, L., Jonckheere, R., Enkelmann, E., Khan, J., Sonntag, B.-L., et al. (2016). Cenozoic intracontinental deformation and exhumation at the northwestern tip of the India-Asia collision–southwestern Tian Shan, Tajikistan, and Kyrgyzstan. *Tectonics*, *35*, 2171–2194. https://doi.org/10.1002/2015tc003897

Kretz, R. (1983). Symbols for rock-forming minerals. *American Mineralogist*, *68*, 277–279.

Kylander-Clark, A. R. C., Hacker, B. R., & Cottle, J. M. (2013). Laser-ablation split-stream ICP petrochronology. *Chemical Geology*, *345*, 99–112. https://doi.org/10.1016/j.chemgeo.2013.02.019

Linnemann, U., Ouzegane, K., Drareni, A., Hofmann, M., Becker, S., Gärtner, A., & Sagawe, A. (2011). Sands of west Gondwana: An archive of secular magmatism and plate interactions—A case study from the Cambro-Ordovician section of the Tassili Ouan Ahaggar (Algerian Sahara) using U-Pb-LA-ICP-MS detrital zircon ages. *Lithos*, *123*, 188–203. https://doi.org/10.1016/j.lithos.2011.01.010

Ludwig, K. R. (2000). *SQUID 1.00, A User's Manual* (Vol. 2). Berkeley Geochronology Center Special Publication.

Paton, C., Hellstrom, J. C., Paul, B., Woodhead, J. D., & Hergt, J. M. (2011). Iolite: Freeware for the visualisation and processing of mass spectrometer data. *Journal of Analytical Atomic Spectrometry*, *26*, 2508–2518. https://doi.org/10.1039/c1ja10172b

Pfänder, J. A., Sperner, B., Ratschbacher, L., Fischer, A., Meyer, M., Leistner, M., & Schaeben, H. (2014). High-resolution $^{40}Ar/^{39}Ar$ dating using a mechanical sample transfer system combined with a high-temperature cell for step heating experiments and a multi-collector ARGUS noble gas mass spectrometer. *Geochemistry, Geophysics, Geosystems*, *15*, 2713–2726. https://doi.org/10.1002/2014gc005289

Powneby, M.-I., Wall, V.-J., & O'Neill, H. S. C. (1987). Fe-Mn partitioning between garnet and ilmenite; experimental calibration and applications. *Contributions to Mineralogy and Petrology*, *97*(1), 116–126. https://doi.org/10.1007/bf00375219., .

Rutte, D., Pfänder, J. A., Koleška, M., Jonckheere, R., & Unterricker, S. (2015). Radial fast-neutron fluence gradients during rotating $^{40}Ar/^{39}Ar$ sample irradiation recorded with metallic fluence monitors and geological age standards. *Geochemistry, Geophysics, Geosystems*, *16*, 336–345. https://doi.org/10.1002/2014gc005611

Rutte, D., Ratschbacher, L., Khan, J., Stübner, K., Hacker, B. R., Stearns, M. A., et al. (2017). Building the Pamir-Tibet Plateau—Crustal stacking, extensional collapse, and lateral extrusion in the Central Pamir: 2. Timing and rates. *Tectonics*, *36*, 385–419. https://doi.org/10.1002/2016tc004294

Spear, F. S. (1993). *Metamorphic phase equilibria and pressure-temperature-time paths* (p. 799). Mineralogical Society of America Monographs.

Stübner, K., Ratschbacher, L., Weise, C., Chow, J., Hofmann, J., Khan, J., et al. (2013). The giant Shakhdara migmatitic gneiss dome, Pamir, India-Asia collision zone: 2. Timing of dome formation. *Tectonics*, *32*(5), 1404–1431. https://doi.org/10.1002/tect.20059

Thomas, J. B., Watson, E. B., Spear, F. S., Shemella, P. T., Nayak, S. K., & Lanzirotti, A. (2010). TitaniQ under pressure: The effect of pressure and temperature on the solubility of Ti in quartz. *Contributions to Mineralogy and Petrology*, *160*, 743–759. https://doi.org/10.1007/s00410-010-0505-3

Wauschkuhn, B., Jonckheere, R., & Ratschbacher, L. (2015). The KTB apatite fission-track profiles: Building on a firm foundation? *Geochimica et Cosmochimica Acta*, *167*, 27–62. https://doi.org/10.1016/j.gca.2015.06.015

Wiedenbeck, M., Alle, P., Corfu, F., Griffin, W. L., Meier, M., Oberli, F., et al. (1995). Three natural zircon standards for U-Th-Pb, Lu-Hf, trace element and REE analyses. *Geostandards Newsletter*, *19*, 1–23. https://doi.org/10.1111/j.1751-908x.1995.tb00147.x

Williams, I. S. (1998). U-Th-Pb geochronology by ion microprobe. *Reviews in Economic Geology*, *7*, 1–35.